

# Metabolic pathway and distribution of superparamagnetic iron oxide nanoparticles: in vivo study

Eva K Schlachter<sup>1</sup>  
Hans Ruedi Widmer<sup>1</sup>  
Amadé Bregy<sup>1</sup>  
Tarja Lönnfors-Weitzel<sup>2</sup>  
Istvan Vajtai<sup>3</sup>  
Nadia Corazza<sup>3</sup>  
Vianney JP Bernau<sup>6</sup>  
Thilo Weitzel<sup>2</sup>  
Pasquale Mordasini<sup>2</sup>  
Johannes Slotboom<sup>2</sup>  
Gudrun Herrmann<sup>4</sup>  
Serge Bogni<sup>5</sup>  
Heinrich Hofmann<sup>6</sup>  
Martin Frenz<sup>5</sup>  
Michael Reinert<sup>1</sup>

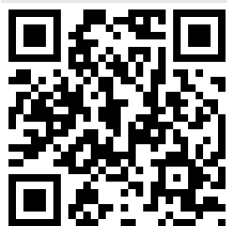
<sup>1</sup>Department of Neurosurgery,

<sup>2</sup>Institute for Diagnostic and Interventional Neuroradiology,

<sup>3</sup>Department of Pathology, <sup>4</sup>Institute of Anatomy, <sup>5</sup>Institute of Applied Physics, University of Bern, Berne, Switzerland;

<sup>6</sup>Laboratory of Powder Technology, Ecole Polytechnique Fédérale de Lausanne, Lausanne, Switzerland

→ Video abstract



Point your smartphone at the QR code to the left. If you have a QR code reader the video abstract will appear. Or use: <http://dvpr.es/reinert>

Correspondence: Michael Reinert  
Department of Neurosurgery, Inselspital  
Bern, 3010 Berne, Switzerland  
Tel +41 31 632 2486  
Fax +41 31 382 2414  
Email [mmv.reinert@insel.ch](mailto:mmv.reinert@insel.ch)

**Background:** Experimental tissue fusion benefits from the selective heating of superparamagnetic iron oxide nanoparticles (SPIONs) under high frequency irradiation. However, the metabolic pathways of SPIONs for tissue fusion remain unknown. Hence, the goal of this in vivo study was to analyze the distribution of SPIONs in different organs by means of magnetic resonance imaging (MRI) and histological analysis after a SPION-containing patch implantation.

**Methods:** SPION-containing patches were implanted in rats. Three animal groups were studied histologically over six months. Degradation assessment of the SPION-albumin patch was performed in vivo using MRI for iron content localization and biodistribution.

**Results:** No SPION degradation or accumulation into the reticuloendothelial system was detected by MRI, MRI relaxometry, or histology, outside the area of the implantation patch. Concentrations from 0.01 µg/mL to 25 µg/mL were found to be hyperintense in T1-like gradient echo sequences. The best differentiation of concentrations was found in T2 relaxometry, susceptibility-sensitive gradient echo sequences, and in high repetition time T2 images. Qualitative and semiquantitative visualization of small concentrations and accumulation of SPIONs by MRI are feasible. In histological liver samples, Kupffer cells were significantly correlated with postimplantation time, but no differences were observed between sham-treated and induction/no induction groups. Transmission electron microscopy showed local uptake of SPIONs in macrophages and cells of the reticuloendothelial system. Apoptosis staining using caspase showed no increased toxicity compared with sham-treated tissue. Implanted SPION patches were relatively inert with slow, progressive local degradation over the six-month period. No distant structural alterations in the studied tissue could be observed.

**Conclusion:** Systemic bioavailability may play a role in specific SPION implant toxicity and therefore the local degradation process is a further aspect to be assessed in future studies.

**Keywords:** superparamagnetic iron oxide nanoparticles, metabolism, distribution

## Introduction

Applications of superparamagnetic iron oxide nanoparticles (SPIONs) in medical diagnosis and therapy are based on two major advantages of iron oxides, ie, their low toxicity to human beings and their strong interaction with high frequency electromagnetic fields.<sup>1</sup> Therefore, SPIONs have gained wide clinical acceptance in diagnostic radiology practice because they cause inhomogeneous susceptibility in magnetic resonance imaging (MRI) and change the relaxometry curves. However, their therapeutic applications in drug delivery, cell labeling, and tissue engineering are still under investigation.<sup>2</sup> In addition, SPIONs can be used in minimally invasive sutureless surgery or hyperthermia, eg, in glioma therapy.<sup>3,4</sup> In contrast with commonly

used laser soldering techniques, electromagnetic tissue soldering has the advantages of being free of practically any energy attenuation, while depositing energy and passing the tissue. Although SPION electromagnetic tissue soldering is possible, the metabolism and long-term effects on tissue of extracellularly deposited SPIONs is not yet tested. In contrast, the biodistribution of SPIONs used as an intravenous contrast agent for MRI is widely studied.<sup>2,5</sup> Tissue distribution is mainly influenced by particle size, whereby larger SPIONs (over 50 nm in diameter) tend to rely on passive targeting, such as uptake by the reticuloendothelial system, and the smaller SPIONs (under 50 nm) benefit from slower opsonization and clearance from the reticuloendothelial system.<sup>6</sup> In addition to particle size, the rate of hepatic clearance of SPIONs depends on the coating material used on the iron oxide particles.<sup>7</sup> Biodistribution, pharmacokinetics, and possible toxicity depend on properties such as particle size, surface morphology, and surface charge.<sup>8</sup> In general, smaller particles circulate for longer than larger particles, and can be gradually taken up by the reticuloendothelial system in lymph tissue and bone marrow.<sup>8–13</sup> Larger particles over 50 nm are generally taken up quickly by the reticuloendothelial system in Kupffer cells of the liver, and have limited uptake in lymph and bone tissues.<sup>6</sup> The coating material rather than the mean hydrated size of the iron oxide particle contributes significantly to the rate of iron oxide particle clearance and degradation in sinusoidal Kupffer liver cells, especially for particles smaller than 40 nm in diameter.<sup>7</sup> Overall, iron oxide particles with coating materials which limit or hinder water access to the core exhibit significantly longer degradation rates, as reflected by the increased half-life of these particles in the liver.<sup>7</sup> No toxic effects have been reported for these hydrated SPION contrast agents. In addition to size and surface coating, the surface charge of SPIONs plays a critical role in their half-life in blood. Positively charged particles tend to adhere nonspecifically to cells.<sup>14</sup> Strong negative charges on the surface are also detrimental in that they result in increased liver uptake.<sup>7</sup> In a recently published report, Hanani et al demonstrated that uncoated chemically engineered iron oxide nanoparticles can have harmful effects in the liver, kidney, and lungs when administered by a single intravenous injection.<sup>15</sup>

When using SPIONs for tissue soldering, their specific size needs to be assessed for optimal heating capability, because these SPIONs can be “tuned” with their corresponding electromagnetic frequency, also referred to as Néel and Brownian relaxation.<sup>16</sup> To generate a temperature of 80°C–100°C necessary for strong and tight tissue fusion at a constant flux of

40 mT for 60 seconds, the size of the SPIONs should be about 15 nm.<sup>17</sup> The uncoated SPIONs were mixed with albumin in a semidry formulation as used for tissue soldering. No toxic effect from albumin on local cellular levels after ingestion has been reported in fibroblasts.<sup>18</sup>

The objective of this study was to analyze specific SPIONs for use in tissue soldering and to find the possible pathways of the SPIONs in question from the site of implantation.<sup>3</sup> Therefore, SPIONs were tracked using a magnetic resonance tracking method as well as histological assessment of the organs involved in degradation and excretion. Kuhlper et al reported recently that SPIONs can be detected, even in minute concentrations.<sup>19</sup> We aimed to quantify these concentrations in an *in vitro* dilution series. The potential toxic effects elicited by iron oxide nanoparticles are addressed in the discussion.

## Materials and methods

Local resorption of SPIONs after subcutaneous implantation of a SPION-albumin patch and the effect on remote organs were evaluated over a six-month period *in vivo* in three animal groups. SPION tracking was performed using MRI, histology, and transmission electron microscopy (TEM) to assess for the presence of SPIONs in selected organs. Prior to the *in vivo* experiments, a MRI tracking dilution series was performed *in vitro* to assess the limit of detection.

## MRI investigations

All imaging was performed in a 3.0 Tesla scanner (Trio TIM, Siemens, Erlangen, Germany) with a 12-channel head coil. While T2\* relaxometry is known to show better contrast compared with T2 relaxometry, the T2\* relaxometry is more sensitive to cell-bound SPIONs than to free SPIONs.<sup>19</sup> T2 relaxometry was preferred for semiquantitative measurements of both intracellular and extracellular SPION concentrations in tissue. Relaxometry was performed using a multicontrast spin echo sequence (repetition time 1500; echo time 12 msec to 96 msec in steps of 12 msec). The signal decay was calculated for each pixel assuming a monoexponential decay function  $S(TE, \text{echo time}) = A \exp(-TE/T_2)$ , where A = signal amplitude, which was normalized to 1 before application of a least square fit algorithm. The first value of each sequence measured at TE = 12 msec was omitted due to artifacts caused by the pulse sequence.<sup>20</sup> Statistics were calculated using Excel® (Microsoft Corporation, Redmond, WA).

## In vitro dilution series

Before *in vivo* assessment of iron by the MRI scanner, an *in vitro* dilution series of 0.01 µg/mL to 5 mg/mL was performed

to detect concentration-dependent susceptibility changes and to assess the lowest detectable level of SPION concentration. Different concentrations (0.01 µg/mL to 5 mg/mL) of uncoated Fe<sub>2</sub>O<sub>3</sub> SPIONs (15 nm in diameter) were prepared in agarose and quantitatively analyzed in a 3 Tesla MRI (Trio TIM, Siemens) for signal alteration (T2 relaxometry using a multicontrast spin echo sequence and R2\*.<sup>21</sup>) The region of interest for measurement in the sample tubes was set into the middle of the test tube to avoid partial volume effects.

## In vivo experiments

### SPION-albumin complex

A water-based suspension of Fe<sub>2</sub>O<sub>3</sub> SPIONs with a particle diameter of 15 nm in combination with bovine serum albumin was used. The solder consisted therefore of 20% (w/w) bovine serum albumin (Cohn Factor V, Sigma Aldrich, Switzerland) dissolved in pure sterile water and mixed in a waterbath at 37°C. The solder was then blended with the dissolved SPIONs (20% w/w), and dispersed in a Petri dish, and allowed to air-dry in order to obtain an implantable solder patch. Patches of 400 µm thickness were rolled and then cut using a predefined square cutter of 25 mm<sup>2</sup>. The weight of these patches was 27.2 ± 0.3 mg, corresponding to 5.52 ± 0.07 mg of ferric oxide per patch. This resulted in a volume of 10 mm<sup>3</sup> per patch and a Fe<sub>2</sub>O<sub>3</sub> concentration of 552 mg/mL.

### Animals

Twenty-five adult male Wistar rats weighing 300–360 g were included in the study. The experiments were performed with the approval of the Ethics Committee for Animal Experiments at the Canton of Bern, Switzerland. The study design consisted of three groups, ie, group A, which had SPION-albumin patch implantation followed by induction-based heating (n = 8), group B, which had SPION-albumin patch implantation without induction heating (n = 8), and group C,

which was a sham control group (n = 9), the latter being included to distinguish iron degradation from postoperative hematoma and MRI artifacts. After anesthesia, the animal's skull was shaved, a transverse incision of approximately 1 cm was made in the nuchal midline, and a small 1 cm pouch was prepared. In groups A and B, the implant was placed subcutaneously inside this small pouch. The incision was then closed using 4–0 Vicryl sutures (Ethicon, Johnson and Johnson, Schaffhausen, Switzerland) and disinfected. The animals were then returned to the animal facility, and their behavior and food intake were observed postoperatively.

MRI tracking was conducted for six months at several time points, ie, days 1, 3, and 15, week 4, and months 3 and 6. The regions of interest in the different measurement sites (liver, kidney, nucleus caudatus) were fixed in an image where anatomical structure was best delineated, then copied into the same position at other echo times in order to achieve identical voxels for measurement.

### Induction heating

The animals in Group A were subjected to induction heating of the SPION-albumin patch after implantation as previously reported.<sup>22</sup> Briefly, a high frequency generator (Power Controller 32/1800, Ceia, Arezzo, Italy) was used, operating at a constant frequency of 1.8 MHz and a constant flux of 40 mT. The coil was placed on the skin, 1–2 mm from the implant. The implant was induced for 60 seconds until a temperature of 80°C was reached.<sup>22–24</sup>

### Histological and ultrastructural analysis

Following MRI assessment, all animals were sacrificed and histologically analyzed (Table 1). The main area for histological analysis was the local SPION-albumin patch implant area and SPION metabolism and distribution in organs, such as liver, pancreas, kidney, brain, and spleen. Immediately after

**Table 1** Histology and TEM results for all animals by treatment group at all study time points

Time	Group A		Group B		Group C		Total
	With TEM	Without TEM	With TEM	Without TEM	With TEM	Without TEM	
1 day	1	–	1	–	–	1	3
3 days	–	1	–	1	–	–	2
15 days	–	1	–	1	–	–	2
4 weeks	1	–	1	–	–	1	3
3 months	–	2	–	2	–	2	6
6 months	1	1	1	1	–	5	9
Total	3	5	3	5	0	9	25

**Notes:** Histological analysis to measure iron concentrations in organs (liver, kidney, pancreas, brain) and local implantation area. MRI done in whole-body scan with regions of interest set at brain (nucleus caudatus), liver, and kidney. TEM was performed in groups A and B after day 1, week 4, and month 6. TEM analysis of the sham-operated group (group C) was not performed.

**Abbreviations:** MRI, magnetic resonance imaging; TEM, transmission electron microscopy.

removal from the cadavers, tissue samples were fixed overnight in a 5% buffered aqueous solution of formaldehyde (Pharmacy Inselspital, Bern, Switzerland), and routinely processed in paraffin. Consecutive serial sections of 3  $\mu\text{m}$  thickness were alternately stained with hematoxylin and eosin and Prussian Blue. All sections were examined under light microscopy in a diagnostic surgical pathology setting. Hematoxylin and eosin and Prussian Blue staining was performed at all time points.

To detect apoptotic cells we performed immunohistochemical analyses for caspase-3 at three days and six months. For this purpose, two different primary antibodies and consequently two different staining protocols were used as follows. In the first protocol, sections were deparaffinized and then blocked by 0.1% Triton X-100 in phosphate-buffered saline plus 10% normal goat serum for 60 minutes, washed, and incubated overnight with the primary antibody (affinity purified polyclonal rabbit antiactive caspase-3 antibody, 1:1000, Promega, Madison, WI) with 0.1% Triton X-100 in phosphate-buffered saline plus 2.5% horse serum at 4°C. Bound antibodies were visualized using the Vectastain method (Vector Laboratories) in combination with a metal-enhanced 3,3'-diaminobenzidine substrate kit as previously described.<sup>26</sup> In the second protocol, after deparaffinization, the sections were incubated in primary antibodies (monoclonal rabbit anticlaved caspase-3 antibody, 1:100, Cell Signaling Technology, Beverly, MA) in phosphate-buffered saline containing 5% normal goat serum and 0.5% casein for 60 minutes.<sup>25</sup> Sections were then treated as described above, dehydrated in alcohol, cleared in xylene, and mounted in Eukitt. Staining control adjacent sections were incubated in the absence of primary antibodies. In addition, cultured striatal cells exposed to 3-nitropropionic acid served as positive controls for caspase-3 staining.<sup>27</sup> TEM was performed on specimens of the SPION-albumin patch implant area and the liver after day 1, week 4, and month 6 (groups A and B). No samples were analyzed in the sham-operated animals (group C).

## Results

### MRI in vitro dilution series

Susceptibility changes were demonstrated in all probes examined. Concentrations from 0.05  $\mu\text{g}/\text{mL}$  to 25  $\mu\text{g}/\text{mL}$  were found to be hyperintense in T1-like gradient echo sequences and increasingly hypointense in concentrations up to 5 mg/mL. The best differentiation of concentrations was found in T2 relaxometry values, susceptibility sensitive gradient echo sequences, and in high repetition time T2 images, in accordance with a method previously published by Kuhlper

et al.<sup>19</sup> In tissue-like environments, the detection limit was established for SPIONs by using T2 relaxometry effective down to 2.5  $\mu\text{g}/\text{mL}$ .

### Animal outcomes

All animals ( $n = 25$ ) showed normal food intake and growth during the study period. All animals survived surgery, and the following MRI studies and observation period (Table 1).

### MRI in vivo

MRI showed signal alterations in the implantation area throughout the observation period (day 1, day 3, day 15, week 4, and months 3 and 6). Imaging and analysis of the regions of interest in the corresponding organs (liver, kidney, nucleus caudatus) gave no indication of altered T2 decay times due to diffuse and detectable concentrations of SPIONs. Figure 1 shows the primary regions of interest analyzed in each animal. The relaxation curves for the kidney, liver, and nucleus caudatus showed normal decay, with no divergent values due to iron accumulation. Figure 2 shows the half-life periods for the treated animals compared with mean values for the control group.

### Histological findings

None of the organs studied (brain, liver, spleen) showed either direct evidence of excessive iron accumulation or tissue alterations suggestive of iron overload. Liver changes in the form of increased numbers of Kupffer cells were found, but were identical in SPION-treated and sham-operated animals. This was most likely due to the trauma of surgery (Figure 3). At the implant site itself, the inflammatory exudate tended to be more granulocyte-rich in the absence of electromagnetic heating, whereas mononuclear cells (lymphocytes and macrophages) were predominant near the heat pretreated

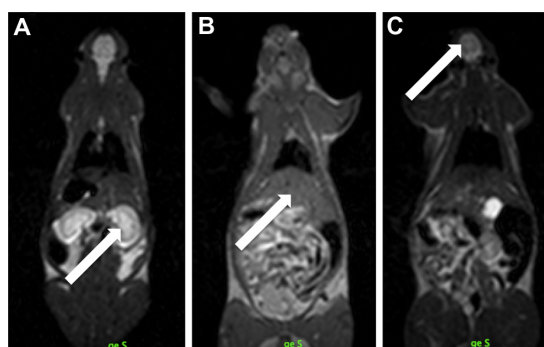


**Figure 1** Three full-body magnetic resonance scans in a rat. After choosing a suitable slice position for each rat, standardized regions of interest are placed in homogenous parts of (A) kidney, (B) liver, and (C) nucleus caudatus (marked with arrows) to measure and compare T2 relaxation times.

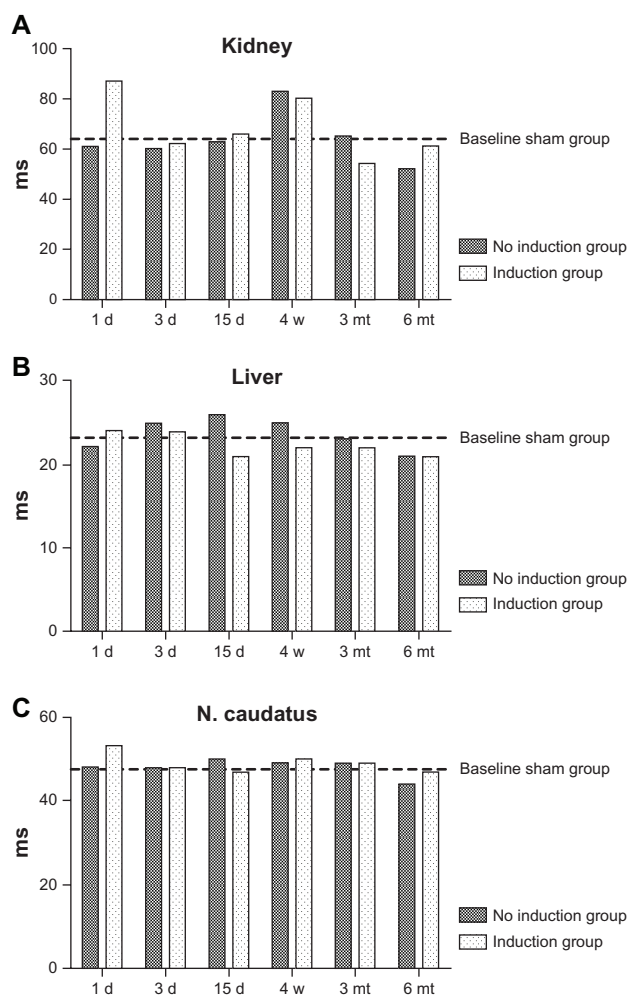


**Figure 2** Comparison of the half-life values in milliseconds of the decay curves in all tested (A) livers, (B) kidneys, and (C) nucleus caudatus of animals with implanted patches. For better visualization, the mean values for the sham-operated group is marked as a bar. The values show no systematic variation, regardless of whether a sham-operated, induction, or no induction group. Variation of values in the kidney is probably a normal phenomenon caused by nonhomogeneous regions of interest regarding the constantly changing water content. The same amplitude of variation can be found in the sham group.

(soldered) implants. In the late phases of the observation period, the implant site tended to be largely organized by fibrous remodeling with no significant foreign body reaction. The SPION-albumin complex was slowly reabsorbed over the observation period (Figures 4 and 5). Both active caspase-3 and cleaved caspase-3 apoptosis staining at day 3 and month 6 occasionally showed some positive cells in the liver and local implant site, but no difference was observed between sham and treated animals (Figures 3 and 4).

### Ultrastructural findings

TEM revealed that parts of the SPION-derived iron granules were engulfed by macrophages at the implantation site.

No toxic effects caused by the SPIONs were demonstrated (Figure 6). In the liver, the selective storage of iron within the cytoplasm of Kupffer cells was assessed as normal physiological activity (Figure 7).

### Discussion

SPIONs in general may have different size and conformation status such as is seen in contrast agents, in contrast with hyperthermia and soldering situations. In this study, the SPIONs used for heating were prepared as single particles in an aqueous solution together with albumin. The histological and TEM images obtained from the subcutaneously implanted SPION-albumin complexes showed rather compact aggregates. The edges of the implant were exposed to slow degradation (Figure 5). TEM images showed intracellular aggregates of SPIONs, meaning that the distribution of the SPIONs did not follow the same clearance stages as described for SPIONs used as contrast agents. Intravascularly injected SPIONs were mainly found in the reticuloendothelial system of the liver. Furthermore, using MRI tracking, we were not able to detect any SPIONs or R2 changes in any of the observed organs, down to a concentration lower than 2.5  $\mu\text{g}/\text{mL}$ . Histological assessment, as well as TEM sections of the liver, was in accordance with these MRI findings, and showed no SPION-induced effect in comparison with the control group.

The amount of iron released by the SPION-albumin patch, in respect to systemic resorption, is so low that from this standpoint no toxic effects are expected. Adult humans ingest about 12–18 mg of dietary iron per day, and the mucosa alone absorbs about 1–2 mg per day.<sup>28</sup> The maximum dose of iron released by the SPION-albumin patch using the amount of iron per patch (5.52 mg) corresponds to about double the daily dietary ingestion by a human adult. In a rat, this corresponds to about 36 times the dietary intake of iron per day (roughly 150  $\mu\text{g}$  Fe).<sup>29</sup> However, this is a single implant absorbed slowly over a period of more than six months. The implant is still present although diminished to about half of its initial configuration after more than 180 days. This would correspond to about an average of 15  $\mu\text{g}$  Fe per day. As reported, histological and TEM analysis showed no toxic effect during the six-month study period. However, there was a small increase in Kupffer cells in the liver to be addressed, which corresponds to normal development over time, given that it was also observed in the sham-operated group and has been described in the literature in aging rats.<sup>30</sup>

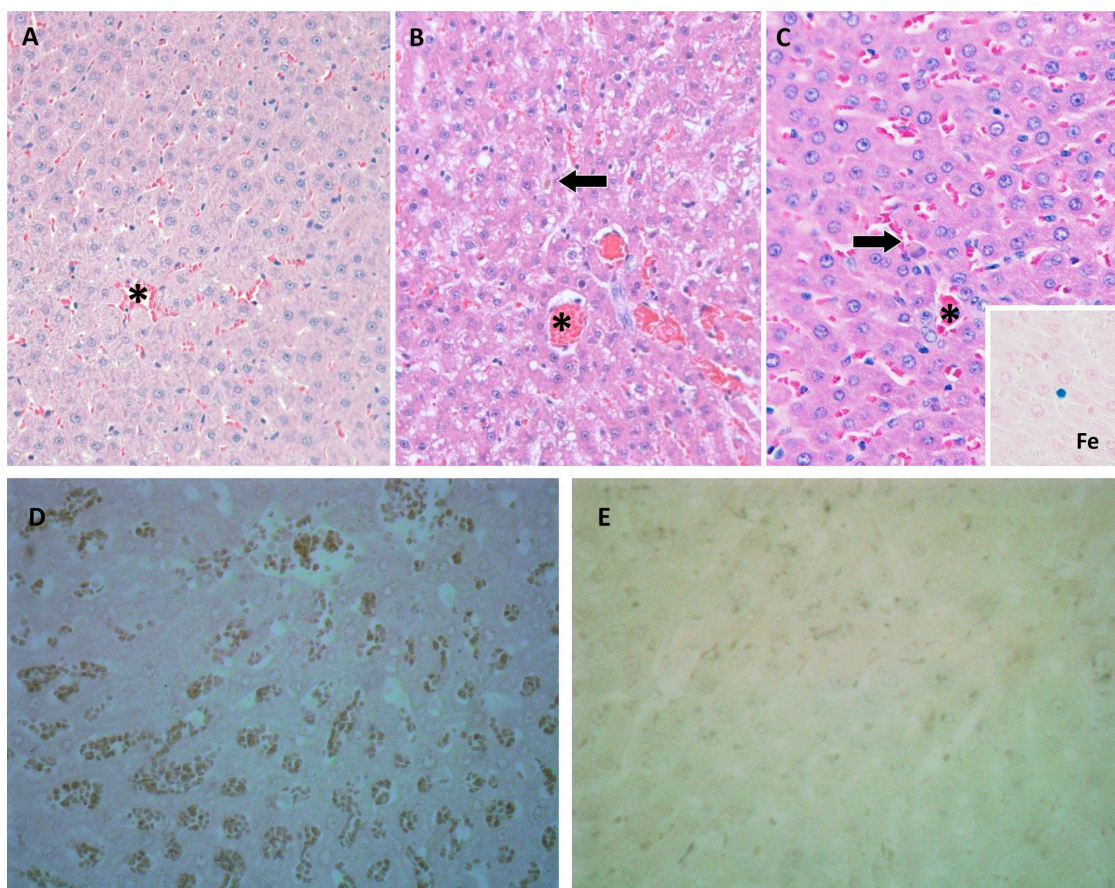


**Figure 3** Conventional light microscopic histology of representative rat liver tissue removed (A) three days and (B) six months after implantation of superparamagnetic iron oxide nanoparticles. (C) Liver tissue of a sham-treated animal after six months. All visual fields include a central vein. Neither iron storage in hepatocytes nor fibrosis is seen. Arrows in (B) and (C) point to minute iron deposits in a Kupffer cell flanking a sinusoid. This chance finding is due to age-related increase of Kupffer cells and is therefore less likely to be encountered in young animals. (A) Iron granules are readily distinguished from lipofuscin pigment using Prussian Blue staining (inset in C). Slides not labeled otherwise represent hematoxylin and eosin staining; original magnification 200 $\times$ . Representative section of rat liver using active caspase-3 antibody staining at three days (D) 40 $\times$  and cleaved caspase-3 antibody staining at six months (E) 40 $\times$  demonstrated no apoptotic activity. Sham caspase is not shown because no difference was detected.

In general, a foreign body giant cell formation from the fusion of macrophages has been observed as a result of the response induced by biomaterials and other foreign bodies, and we also found this in our study.<sup>31</sup> The size and surface characteristics of these giant cells elicit a prolonged series of reactions, a process known as the foreign body response.<sup>31</sup> Although inflammation and macrophage activation resolve in the later stages of wound healing to promote tissue remodeling, the foreign body response is characterized by persistence of inflammatory cells, particularly macrophages, at the site of implantation. On the implant surface, macrophages fuse into multinucleated giant cells. In comparison with single macrophages, giant cells are capable of delivering a more effective and concentrated assault on the implant, degrading material and even causing failure of implanted devices. The presence of giant cells was also observed in the implants used in our study, with a progressive degradation of the

SPION implant over the six-month observation period, further undermining the low toxicity and iron systemic iron load over time.

Results differing from ours were recently published by Hanini et al, who demonstrated a toxic effect in the liver, kidney, and lungs after intravenous injection of 0.8 mg of iron oxide nanoparticles.<sup>15</sup> In our study, we did not observe toxic effects because our SPIONs-containing implants did not induce structural changes in the liver and kidney, and also did not increase apoptosis as compared with controls. One possible explanation for this discrepancy in outcome may be the way in which the nanoparticles were released into the system. Slow degradation of the implant with the described foreign body response may be responsible for the slow systemic availability. A detailed quantification of this process up until complete resorption of the implant needs to be performed to elucidate this question fully.

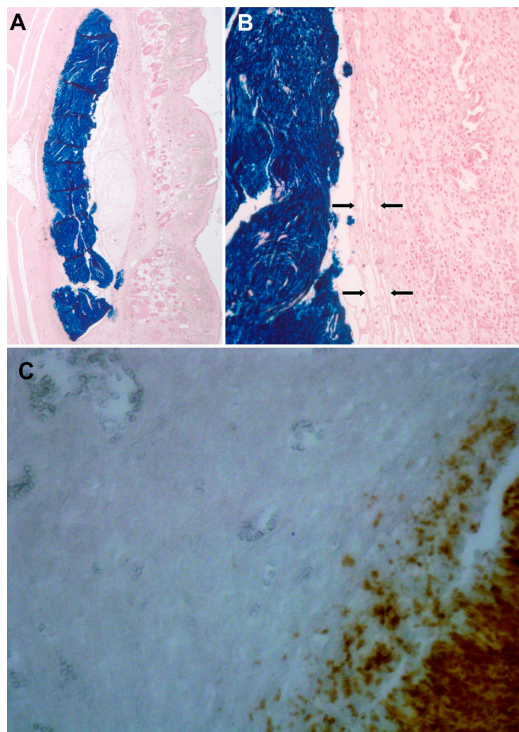


**Figure 4** Histological findings of the superparamagnetic iron oxide nanoparticle-albumin complex three days after implantation and heat treatment in an electromagnetic field for 60 seconds. (A) Scanning magnification shows implant smoothly accommodated along the cleavage plane of subcutaneous fascia and axial musculature with no significant space-occupying effect. (B) Detailed view of implant/tissue interface indicates this to consist of a narrow rim of fibrinoid exudate (arrows) surrounded by granulation tissue. Prussian Blue staining; original magnification (A) 15 $\times$  and (B) 100 $\times$ . In (C), active caspase-3 antibody staining shows no apoptotic activity around the implant (40 $\times$ ). Sham not shown because no difference was detected.

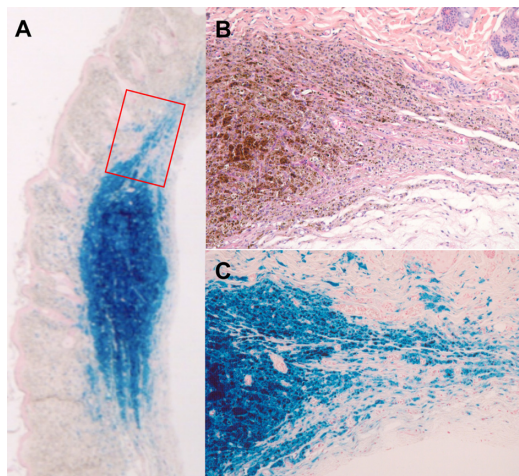


**Figure 5** Histological aspect of superparamagnetic iron oxide nanoparticle-albumin complex in situ six months after implantation and heating procedure. (A) At scanning magnification of Prussian Blue-stained section, centrifugal fading rather than sharp circumscription of implant contours is seen (especially as opposed to Figure 7A). (B) and (C) represent consecutive section planes of boxed area in (A) to indicate gradual dissolution of implant iron content by macrophages. In parallel, there is fibroblastic ingrowth. Note absence of significant foreign body reaction. (A) and (C) Prussian Blue staining, (B) hematoxylin and eosin staining; original magnifications (A) 15 $\times$  and (B) and (C) 200 $\times$ .

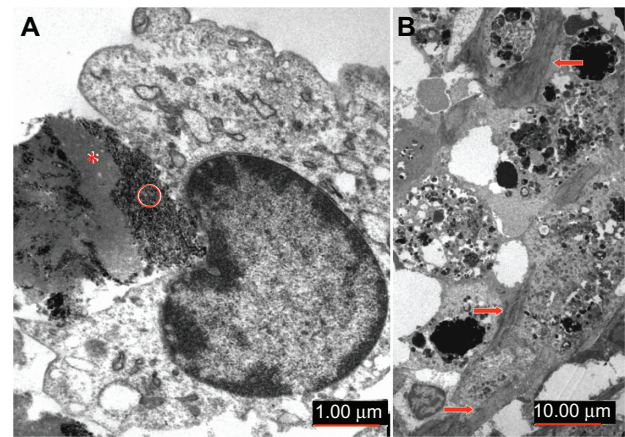


**Figure 6** Ultrastructural aspect of implant/tissue interaction as seen on transmission electron microscopy. (A) Detailed view of early phase of implant degradation showing ongoing engulfment of the superparamagnetic iron oxide nanoparticles-albumin complex by activated monocytes. Heterogeneous electron density of implant material is seen, with electron-lucent zones corresponding to coagulated albumin (\*) whereas dense granules represent iron nanoparticles (O). (B) Organizing phase of implant scavenging is characterized by phagocytic cells replete with electron-dense iron particles. Note intercellular deposition of connective tissue fibers (arrows). Original magnification is indicated by scale bars.

Our findings support the further development of SPIONs designed for inducing hyperthermia or tissue soldering in vivo and local application, first by the lack of R2 signal changes globally and in specific organs, excluding any SPIONs and iron accumulation. Secondly, light microscopic and TEM histology and apoptosis staining of the excretion-related organs were unaffected by the SPIONs. Systemic availability and specific SPION application may be important in the development of a possible toxic effect, as suggested by the discordant findings of Hanini et al and the outcome seen in the present study. Hence, prior to clinical application in a clinical setting, decomposition of the complete SPION implant

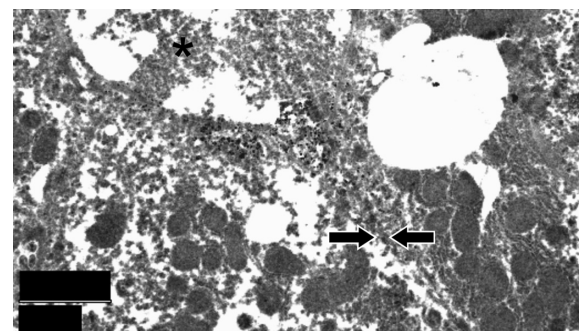


**Figure 7** Ultrastructural aspect of liver from an implant-bearing animal in the late phase of observation period. \*Transected biliary canalicule flanked by two hepatocytes, the cell borders of which (arrows) are not readily identified due to poor specimen preservation. Regular aspect of mitochondria is a good indicator of lack of metabolic stress, as frequently seen in storage disorders. Original magnification is indicated by scale bar.

should be assessed in detail at the site of implantation over a considerable period of time.

## Acknowledgments

We thank Dr A Ducray for support with the immunohistochemical analyses. EKS and AB were supported by a Swiss National Foundation grant, and MR and MF by a Commission for Technology and Innovation project grant.

## Disclosure

The authors report no conflicts of interest in this work.

## References

- Babincova M, Leszczynska D, Sourivong P, Babinec P. Selective treatment of neoplastic cells using ferritin-mediated electromagnetic hyperthermia. *Med Hypotheses*. 2000;54(2):177–179.
- Berry CC. Progress in functionalization of magnetic nanoparticles for applications in biomedicine. *J Phys D Appl Phys*. 2009;42(22):224003.
- Bregy A, Kohler A, Steitz B, et al. Electromagnetic tissue fusion using superparamagnetic iron oxide nanoparticles: First experience with rabbit aorta. *The Open Surgery Journal*. 2008;(2):3–9.
- van Landeghem FK, Maier-Hauff K, Jordan A, et al. Post-mortem studies in glioblastoma patients treated with thermotherapy using magnetic nanoparticles. *Biomaterials*. 2009;30(1):52–57.
- Lacava LM, Lacava ZG, Da Silva MF, et al. Magnetic resonance of a dextran-coated magnetic fluid intravenously administered in mice. *Biophys J*. 2001;80(5):2483–2486.
- Barry SE. Challenges in the development of magnetic particles for therapeutic applications. *Int J Hyperthermia*. 2008;24(6):451–466.
- Briley-Saebo K, Bjornerud A, Grant D, Ahlstrom H, Berg T, Kindberg GM. Hepatic cellular distribution and degradation of iron oxide nanoparticles following single intravenous injection in rats: Implications for magnetic resonance imaging. *Cell Tissue Res*. 2004;316(3):315–323.
- Chouly C, Pouliquen D, Lucet I, Jeune JJ, Jallet P. Development of superparamagnetic nanoparticles for MRI: Effect of particle size, charge and surface nature on biodistribution. *J Microencapsul*. 1996;13(3):245–255.
- Wisner ER, Amparo EG, Vera DR, et al. Arabinogalactan-coated superparamagnetic iron oxide: Effect of particle size in liver MRI. *J Comput Assist Tomogr*. 1995;19(2):211–215.
- Allkemper T, Bremer C, Matuszewski L, Ebert W, Reimer P. Contrast-enhanced blood-pool MR angiography with optimized iron oxides: Effect of size and dose on vascular contrast enhancement in rabbits. *Radiology*. 2002;223(2):432–438.
- Brigger I, Dubernet C, Couvreur P. Nanoparticles in cancer therapy and diagnosis. *Adv Drug Deliv Rev*. 2002;54(5):631–651.
- Gaur U, Sahoo SK, De TK, Ghosh PC, Maitra A, Ghosh PK. Biodistribution of fluoresceinated dextran using novel nanoparticles evading reticuloendothelial system. *Int J Pharm*. 2000;202(1–2):1–10.
- Bartneck M, Keul HA, Zwadlo-Klarwasser G, Groll J. Phagocytosis independent extracellular nanoparticle clearance by human immune cells. *Nano Lett*. 2010;10(1):59–63.
- Fujita T, Nishikawa M, Ohtsubo Y, et al. Control of in vivo fate of albumin derivatives utilizing combined chemical modification. *J Drug Target*. 1994;2(2):157–165.
- Hanini A, Schmitt A, Kacem K, Chau F, Ammar S, Gavard J. Evaluation of iron oxide nanoparticle biocompatibility. *Int J Nanomedicine*. 2011;6:787–794.
- Rosensweig RE. Heating magnetic fluid with alternating magnetic field. *J Magn Magn Mater*. 2002;252:370–374.
- Hilger I, Fruhauf K, Andra W, Hiergeist R, Hergt R, Kaiser WA. Heating potential of iron oxides for therapeutic purposes in interventional radiology. *Acad Radiol*. 2002;9(2):19–202.
- Berry CC, Wells S, Charles S, Curtis AS. Dextran and albumin derivatised iron oxide nanoparticles: Influence on fibroblasts in vitro. *Biomaterials*. 2003;24(25):4551–4557.
- Kuhlperter R, Dahnke H, Matuszewski L, et al. R2 and R2\* mapping for sensing cell-bound superparamagnetic nanoparticles: In vitro and murine in vivo testing. *Radiology*. 2007;245(2):449–457.
- Jones CK. *T2 Decay Curve Acquisition and Analysis in MRI*. Vancouver, Canada: Department of Physics, University of British Columbia; 2003.
- Mordasini P, Lönnfors-Weitzel T. Sequence optimization at 3 Tesla MRI for SPION imaging in the context of tissue soldering. Presented at the annual meeting of the Swiss Society of Neurosurgery. Lugano, Switzerland, October 26–27, 2007.
- Bregy A, Bogni S, Bernau VJ, et al. Solder doped polycaprolactone scaffold enables reproducible laser tissue soldering. *Lasers Surg Med*. 2008;40(10):716–725.
- McNally KM, Sorg BS, Chan EK, Welch AJ, Dawes JM, Owen ER. Optimal parameters for laser tissue soldering. Part I: Tensile strength and scanning electron microscopy analysis. *Lasers Surg Med*. 1999;24(5):319–331.
- Pohl D, Bass LS, Stewart R, Chiu DT. Effect of optical temperature feedback control on patency in laser-soldered microvascular anastomosis. *J Reconstr Microsurg*. 1998;14(1):23–29.
- Jakob S, Corazza N, Diamantis E, Kappeler A, Brunner T. Detection of apoptosis in vivo using antibodies against caspase-induced neo-epitopes. *Methods*. 2008;44(3):255–261.
- Andres RH, Ducray AD, Perez-Bouza A, et al. Creatine supplementation improves dopaminergic cell survival and protects against MPP+ toxicity in an organotypic tissue culture system. *Cell Transplant*. 2005;14(8):537–550.
- Andres RH, Ducray AD, Huber AW, et al. Effects of creatine treatment on survival and differentiation of GABA-ergic neurons in cultured striatal tissue. *J Neurochem*. 2005;95(1):33–45.
- Monsen ER. Iron nutrition and absorption: Dietary factors which impact iron bioavailability. *J Am Diet Assoc*. 1988;88(7):786–790.
- Subcommittee on Laboratory Animal Nutrition, Committee on Animal Nutrition, Board on Agriculture, National Research Council. *Nutrient Requirements of Laboratory Animals*. 4th ed. Washington, DC: National Academies Press; 1995.
- Hilmer SN, Cogger VC, Le Couteur DG. Basal activity of Kupffer cells increases with old age. *J Gerontol A Biol Sci Med Sci*. 2007;62(9):973–978.
- Anderson JM. Inflammatory response to implants. *ASAIO Trans*. 1988;34(2):101–107.

International Journal of Nanomedicine

Publish your work in this journal

The International Journal of Nanomedicine is an international, peer-reviewed journal focusing on the application of nanotechnology in diagnostics, therapeutics, and drug delivery systems throughout the biomedical field. This journal is indexed on PubMed Central, MedLine, CAS, SciSearch®, Current Contents®/Clinical Medicine,

Submit your manuscript here: <http://www.dovepress.com/international-journal-of-nanomedicine-journal>

Dovepress

Journal Citation Reports/Science Edition, EMBase, Scopus and the Elsevier Bibliographic databases. The manuscript management system is completely online and includes a very quick and fair peer-review system, which is all easy to use. Visit <http://www.dovepress.com/testimonials.php> to read real quotes from published authors.